ACS OMEGA

Article

Cite This: ACS Omega 2018, 3, 14097−14102

http://pubs.acs.org/journal/acsodf

Near Infrared Random Lasing in Multilayer MoS_2

Tejendra Dixit,[†,§] Ankit Arora,[†,‡,§] Ananth Krishnan,[‡] K. Lakshmi Ganapathi,[*,†] Pramoda K. Nayak,[*,†] and M. S. Ramachandra Rao[*,†,§]

[†]Department of Physics and Materials Science Research Centre, [‡]Centre for NEMS and Nano Photonics (CNNP), Department of Electrical Engineering, and [§]Nano Functional Materials Technology Centre, Indian Institute of Technology Madras, Chennai 600 036, India

Supporting Information

ABSTRACT: We demonstrated room temperature near infrared (NIR) region random lasing (RL) (800−950 nm), with a threshold of nearly 500 μW, in ∼200 nm thick MoS_2/Au nanoparticles (NPs)/ZnO heterostructures using photoluminescence spectroscopy. The RL in the above system arises mainly due to the following three reasons: (1) enhanced multiple scattering because of Au/ZnO disordered structure, (2) exciton−plasmon coupling because of Au NPs, and (3) enhanced charge transfer from ZnO to thick MoS_2 flakes. RL has recently attracted tremendous interest because of its wide applications in the field of telecommunication, spectroscopy, and specifically in biomedical tissue imaging. This work provides new dimensions toward realization of low power on-chip NIR random lasers made up of biocompatible materials.

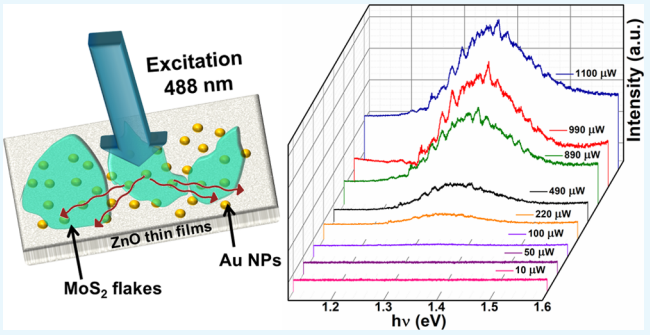

1. INTRODUCTION

Random lasing (RL) is one of the lasing phenomena that arises due to simultaneous action of optical gain and amplification by multiple scattering.[1−3] A random laser is different from a traditional laser in the sense that the feedback amplification is not provided by a cavity formed by reflection components, but by disorder-induced scattering. Because of ease of its fabrication, it is gaining popularity in a variety of applications like biomedical imaging and optical information processing.[2] Use of various plasmonic nanoparticles (NPs) as well as the new class of host materials including semiconductors, quantum dots, and so forth led to renewed interest in the area of random lasers and their applications over last decade.[2,4−6] RL in the spectral range from ultraviolet to visible region has been explored in variety of materials in literature.[4,5,7,8] However, there are few reports about near infrared (NIR) RL so far, which has the following advantages including telecommunication, spectroscopy, displays, and biomedical tissue imaging.[9−11] In addition, because the NIR window of tissue imaging falls in the range 650−1300 nm, NIR lasing using biocompatible materials is extremely needed.

Two-dimensional (2D) transition-metal dichalcogenides (TMDs) have recently attracted significant interest because of their intriguing physical/chemical properties and have huge potential applications in future optoelectronic, nanoelectronic, and spin-valleytronic devices.[12−19] Among the 2D TMDs, molybdenum disulfide (MoS_2) is very promising candidate, which exhibits indirect optical band gap of 1.2 eV in bulk phase to direct band gap of 1.9 eV in monolayer limit.[13,14,20,21] However, the relatively small optical density of states and limited photon absorbing/emitting ability of monolayer MoS_2 restrict its practical device applications.[22−24] The realization of lasing in the visible region has been already reported in monolayer MoS_2.[25,26] As a counterpart of monolayer species, a few layer MoS_2 with thickness <100 nm (TnM) shows low luminescence quantum yield because of their indirect band gap nature. However, thick MoS_2 with thickness >100 nm (TkM) still holds some obvious superiorities compared with monolayer in terms of stronger photon absorption ability, higher optical density of states, and ability to withstand substantially higher injection currents, which are advantageous for light-emitting devices and solar energy conversion.[23,27] Moreover, as MoS_2 is biocompatible and the indirect band gap of TkM lies in the NIR region, it may be possible to build future optoelectronic devices using indirect band gap emission for NIR application.[23,28] However, RL is not possible from MoS_2 alone and needs an additional charge-transfer medium to invoke population inversion.

ZnO exhibits a direct wide band gap (∼3.37 eV) in the UV region and defect-assisted deep level emission in the visible to NIR region and hence is a very suitable material for tunable light emission and photodetection.[29−39] It has been shown that ZnO can be used to tune the optical properties of 1L-TMDs by controlling the charge carrier density.[40] This is due to the fact that the electronic band structures of 1L-TMD/ZnO heterostructure (HS) form the type-II band alignment, where the effective charge transfer occurs at the interface between 1L-TMDs and ZnO that would enhance the photoluminescence

Received: June 8, 2018
Accepted: October 2, 2018
Published: October 25, 2018

(PL) of 1L-TMDs.[40−42] PL enhancement in the visible region has been observed in several such HSs including MoS_2/ZnO and WSe_2/ZnO by considering monolayer or few layer TMDs.[40,43−45] However, to the best of our knowledge, there is no report so far about the indirect band gap PL enhancement using TMD/ZnO HSs.

In this work, we have prepared TkM/ZnO thin film HSs and observed enhanced indirect PL emission of MoS_2. To further enhance the indirect emission, we have incorporated Au NPs at the TkM/ZnO interface and interestingly observed RL in the NIR region. To understand the charge-transfer mechanism and to calculate lasing threshold, we have studied excitation power-dependent PL spectra of TkM/Au/ZnO HSs. On the basis of the above analysis, we have proposed a possible mechanism for lasing in the above system. The demonstration of NIR RL with the integration of MoS_2, Au, and ZnO has potential to open new dimensions toward future optical technologies because of their biocompatibility, ease of fabrication, and on-chip fabrication suitability.

2. MATERIALS AND METHODS

2.1. Synthesis of ZnO Thin Films. A sol−gel process was employed for ZnO thin film deposition on glass substrate. In particular, an equi-molar solution (2 M) of anhydrous zinc acetate and ethanolamine in 2-methoxyethanol was spin coated on the glass substrate at 3000 rpm. Here, ethanolamine has a role of stabilizer. Spin-coated samples were annealed at 250 °C for throwing out organic impurities and improving the adhesion of ZnO thin film with the substrate. The deposition of 5 nm thick Au on these ZnO thin films was subsequently carried out by using dc sputtering system [Quorum (Q-150 RES)]. The thickness of Au coating was measured using inbuilt crystal detectors. UV−visible absorption spectra were recorded by a Cary 60 UV−vis spectrometer (Agilent Technologies) with a range of wavelengths from 200 to 800 nm.

2.2. Preparation of MoS_2 Flakes and TkM/Au/ZnO HSs. High-purity MoS_2 crystal was procured from Graphene Supermarket and mechanically exfoliated on 285 nm SiO_2/Si, ZnO thin film and Au/ZnO to get desired HSs.

2.3. AFM, SEM, PL, and Raman Measurements. Atomic force microscope (AFM) measurement was carried out in tapping mode using Bruker edge dimension system. Scanning electron microscope (SEM) measurements were carried out with Quanta 400 FEG SEM. TnM, TkM, ZnO thin films, Au/ZnO, and TkM/Au/ZnO HSs were investigated using PL and Raman spectroscopy (HORIBA LabRAM). All of the measurements were carried out in a confocal microscopy setup using 488 nm continuous wave laser with spot size ∼1 μm, in which we can readily locate and selectively excite HSs of different layer thicknesses.

3. RESULTS AND DISCUSSIONS

Figure 1a,b shows the room-temperature PL spectra of TnM and TkM flakes transferred on SiO_2/Si substrates (corresponding AFM images are shown in Figure S1). MoS_2 multilayers usually show two distinguishable peaks with peak positions at 1.84 and 1.35 eV.[20,23,46] The peak observed at 1.84 eV with higher intensity corresponds to A direct exciton transition, while the other peak at 1.35 eV with lower intensity can be assigned to the indirect transition (i.e., transition of electrons from I-valley to *K* point).[20,21] In contrast, TkM (thickness of ∼200 nm used in this work) has shown interesting features

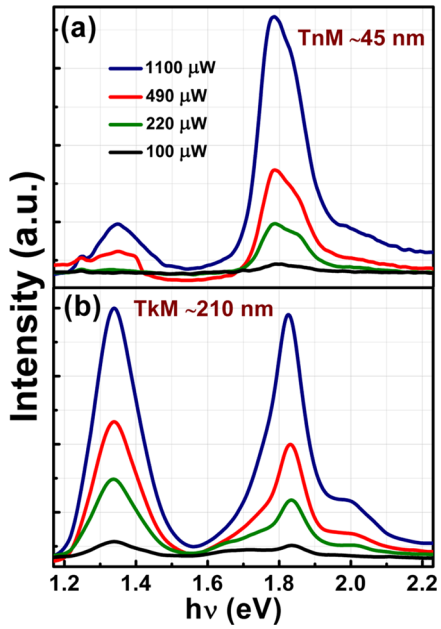

Figure 1. Room temperature PL spectra of MoS_2 flakes on 285 nm SiO_2/Si substrate using 488 nm laser. Excitation power-dependent PL spectra of (a) TnM flakes with thickness ∼45 nm and (b) TkM flakes with thickness ∼210 nm. Black, green, red, and blue colors represent the laser excitation power of 100, 220, 490, and 1100 μW, respectively. Two distinguishable peaks are observed for all flakes, in which peak at 1.84 eV corresponds to direct exciton transition and at 1.35 eV corresponds to indirect transition.

with nearly equal probability for both direct and indirect transitions. Additionally, the B direct exciton transition was observed as a shoulder peak with peak position close to 2.0 eV for both thin and thick flakes. In case of TnM the main excitonic peak can be de-convoluted into two close peaks, that is, A trion and A exciton (see Figure S2). The origin of A^- trion can be attributed to the charge transfer from SiO_2 substrate to MoS_2, which can be clearly seen as a red shift in the A peak position by 15 meV (close to trion binding energy).[47,48] However, for TkM films with thicknesses ∼210 nm, the substrate effect was found to be negligible. The ratio of the peak intensities corresponding to direct and indirect excitonic transitions were observed to be almost invariant with the variation of excitation power. Room-temperature Raman spectra measured on MoS_2 flakes are shown in Figure S3. The Raman spectra of MoS_2 consist of two characteristic peaks at 385 and 405 cm^{-1} corresponding to E_{2g} and A_{1g} modes, respectively.[49] The difference in the Raman shift between these two peaks was found to be ∼25 cm^{-1}, which is in good agreement with the previously reported value for TkM flakes.[49,50] Similar to PL spectra, the peak positions were observed to be invariant for different excitation power. In addition to this, the full-width at half maximum for these peaks monotonically decreased with the decrease in the excitation power.

To investigate the effect of ZnO on MoS_2 flakes, both TnM and TkM were transferred onto sol−gel derived ZnO thin films. The excitation power-dependent PL spectra of TnM/ZnO HSs were observed to be dominated by ZnO emission in the range of 1.6−2.4 eV as shown in Figure S4 and did not show well-defined emission in the NIR region. Therefore, it was not considered for further analysis. On the other hand, the

DOI: 10.1021/acsomega.8b01287
ACS Omega 2018, 3, 14097−14102

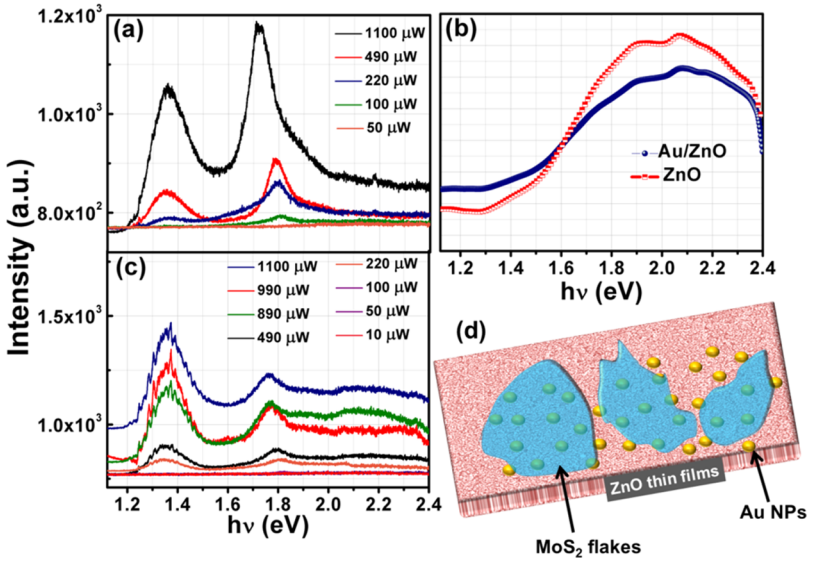

Figure 2. (a) Excitation power-dependent PL spectra of TkM/ZnO HSs showing significant NIR emission. (b) PL spectra of pristine (blue spheres) and Au-coated ZnO thin films (red squares) in the range 1.2−2.4 eV. (c) Excitation power-dependent PL spectra of TkM/Au NPs/ZnO HSs. NIR emission is found to be significantly enhanced along with sharp and narrow peaks over the envelope, which increases with the increase in excitation power. Pink, magenta, purple, orange, black, green, red, and blue colors represent the laser excitation power of 10, 50, 100, 220, 490, 890, 990, and 1100 μW, respectively. (d) Schematic of TkM/Au NPs/ZnO HSs, in which mosaic red represents ZnO thin film, blue flakes represent TkM and golden spheres represent Au NPs.

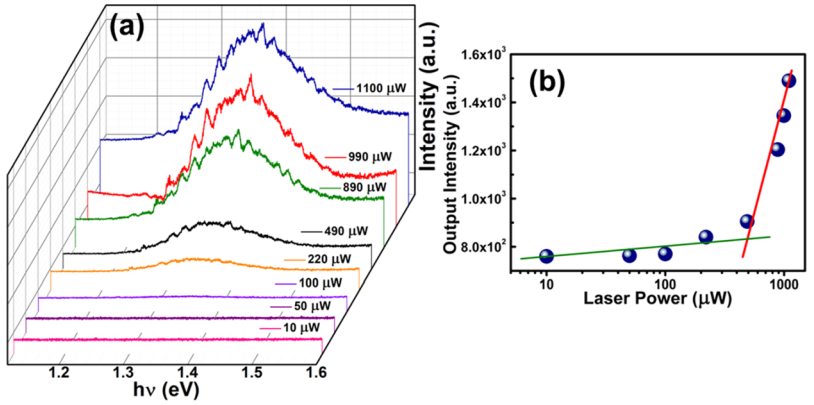

Figure 3. (a) Excitation power-dependent NIR emission of TkM/Au/ZnO HSs. The spectra are plotted in waterfall mode for clarity. Pink, magenta, purple, orange, black, green, red, and blue colors represent the laser excitation power of 10, 50, 100, 220, 490, 890, 990, and 1100 μW, respectively. (b) PL intensity vs excitation power of above HSs. The lasing threshold has been estimated to be ∼500 μW.

PL spectra of TkM/ZnO HSs showed significant NIR emission as shown in Figure 2a. To probe deeper, we recorded the excitation power-dependent PL spectra of TkM/ZnO HSs. The PL spectra of TkM/ZnO HSs showed red shift of direct A transitions in comparison to TkM/SiO_2 films (Figure 1b). MoS_2/ZnO HSs exhibit type-II band alignment and therefore band bending is expected to align the Fermi levels.[41] The conduction band (CB) of MoS_2 followed downward band bending while making an interface with ZnO. Hence, the exciton population of both layers were affected by the charge accumulation at the interface and that made an impact on the ratio of indirect to direct peak values for MoS_2/ZnO HSs. The excitation power-dependent red shift in the position of A exciton peak can be assigned to the photo-induced modulation of MoS_2 dielectric function, thus resulting into the decrease of exciton binding energy.[51] Tuning of A exciton transition of monolayer MoS_2 using ZnO thin film was demonstrated by Kim et al. in MoS_2/ZnO HSs.[40] Figure S5 shows the PL spectrum of TkM/ZnO HS in the region of indirect transition only for laser excitation power of 1100 μW. In contrast to pristine MoS_2 films as mentioned earlier, this HS showed signature of amplified spontaneous emission (ASE) for the transitions related to I-valley as shown in Figure 2a for 1100 μW power (the zoomed spectra corresponding to NIR region is shown in Figure S5). Additionally, the PL spectrum of ZnO thin film is shown in Figure 2b in the range 1.2−2.4 eV, and it was found to be luminescent in the visible and relatively nonluminescent in the region of I-valley of MoS_2. It must be noted here that sol−gel processed ZnO is prone to defect states like oxygen vacancies and interstitials,[52,53] and hence, their interaction with excitonic transitions of MoS_2 cannot be ignored.

The observation of ASE in the indirect exciton transition has triggered its further exploration. It is well known that metal NPs are good candidates for enhancing light scattering mainly because of surface plasmon resonance.[54−56] In the present

DOI: 10.1021/acsomega.8b01287
ACS Omega 2018, 3, 14097−14102

work, we have strategically used Au NPs to get enhanced scattering to have lasing. With the insertion of Au between TkM and ZnO thin films, drastic change in the PL spectra was observed as shown in Figure 2c. The schematic of TkM/Au NPs/ZnO HS is shown in Figure 2d. The corresponding AFM image is shown in Figure S6. Figure S7 shows the typical SEM image of the TkM/Au/ZnO HS. Interestingly, significant enhancement in the emissions corresponding to the I-valley was observed (Figure 2c) along with sharp and narrow peaks over the envelope, which was found to be excitation power dependent. Such features were found to be absent both in pristine MoS_2 and TkM/ZnO HS. In addition, a red shift was observed in the peak corresponding to A direct transitions, which was also found to increase with increase in excitation power.

Figure 3a presents the excitation power-dependent emission in the NIR region of TkM/Au/ZnO HS by varying laser power in the range 10−1100 μW. It was found that the emission intensity increased abruptly beyond excitation power of 490 μW along with the emergence of sharp spike-like peaks over the entire envelope. At lower excitation power (<490 μW), no such sharp peaks were observed. The appearance of the sharp spike-like peaks indicates that RL occurs due to recurrent scattering in the disordered medium of TkM/Au/ZnO. It was observed that the position and intensities of these spike-like peaks were fluctuating for different readings, which is the characteristic of nonresonant feedback.[2] There could be three possible reasons for the origin of such peaks: (1) Fabry−Perot, (2) whispering gallery mode, and (3) RL. As the surface of Au/ZnO is not smooth enough, existence of Fabry−Perot between TkM and Au/ZnO can be neglected. Secondly, whispering gallery mode can also be discarded because of irregular geometry of TkM flakes. Hence, the possible mechanism can be RL only. We have carried out fast Fourier transform analysis for the PL spectra recorded with 1100 μW excitation power. Two side peaks along with the central peak can be clearly seen in the Figure S8, which confirms that the peaks are due to RL and not the noise. The increase in the lasing intensity was found to be nonlinear in nature, as shown in Figure 3b. The change in PL intensity versus excitation power showed an increase in slope indicating the onset of lasing and the lasing threshold was estimated to be approximately 500 μW.

On the basis of the feedback mechanism, RL can be categorized into two types: incoherent when it is phase insensitive and coherent when it is phase sensitive. In a strongly scattering system, multiple scattering facilitates light of wavelength λ to return to the same coherence volume λ^3 it has visited before, thereby providing field feedback for lasing.[6,57,58] The lasing frequencies can be determined by the interference of scattered light returning via different paths.[2] On the basis of the above analysis, we propose the possible mechanism as shown in Figure 4.

As mentioned earlier, band bending at the TkM/ZnO junction results in the charge accumulation in the CB of TkM at the interface. However, the charge accumulation was not sufficient enough for the system to lase. Incorporation of Au NPs between TkM and ZnO resulted in lasing possibly because of three following effects: (1) enhanced multiple scattering, (2) exciton−plasmon coupling, and (3) enhanced charge transfer from ZnO to TkM. It is well reported that plasmon resonance of Au NPs can couple with ZnO excitons (the absorption spectra of ZnO and Au/ZnO is shown in

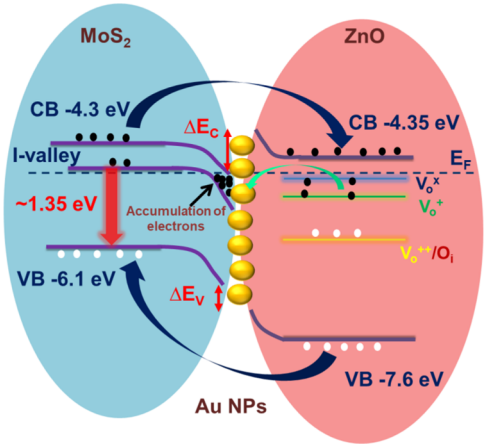

Figure 4. Schematic showing the possible mechanism of RL in TkM/Au/ZnO HSs. Band bending at TkM/ZnO junction results in the charge accumulation in the CB of TkM at the interface, however not sufficient enough for the system to lase. Incorporation of Au NPs (golden spheres) between TkM and ZnO results in lasing possibly due to three following effects, that is, enhanced multiple scattering because of Au/ZnO disordered structure, exciton−plasmon coupling because of Au NPs, and enhanced charge transfer from ZnO to thick MoS_2.

Figure S9; it can be clearly seen that the plasmon resonance peak is present nearly at 528 nm), thereby improving radiative recombination.[59] Because of the difference in work function and electron affinity between ZnO and MoS_2, electrons present in the ZnO may diffuse into TkM at the interface to match the Fermi levels, which can yield depletion region in the ZnO side and a negatively charged carrier accumulation region in the MoS_2 side. Additionally, the presence of Au will promote the band bending and therefore enforce charge accumulation at MoS_2 CB. Electrons present at defect states of ZnO can be transferred to the Au Fermi level and then to MoS_2 CBs, specifically I-valley, as the later is well matched with the Fermi level of Au. For better understanding, we have recorded the PL spectra using 632 nm laser and found no RL which indicates clear involvement of Au NPs for achieving lasing (shown in Figure S10).

Raman spectra for TkM/Au/ZnO HSs are shown in Figure S11. In contrast to Raman spectra of pristine MoS_2 flakes, here a systematic red shift in the peak positions corresponding to E_{2g} and A_{1g} modes was observed. The shift in E_{2g} mode can be assigned to strain induced due to rough ZnO thin films. Moreover, the shift in A_{1g} peak toward lower energy suggests electron transfer from Au/ZnO to TkM.[41,51]

4. CONCLUSIONS

In conclusion, we demonstrated RL action from MoS_2/Au/ZnO HS in the NIR region. Thick-layer MoS_2 flakes were found to be a potential candidate for NIR emission. The thick-layer MoS_2 flakes while transferred onto ZnO thin films resulted in enhanced indirect emission. To enhance the PL emission further, Au NPs were incorporated at the interface between TkM and ZnO. The resulting TkM/Au/ZnO HS was found to lase in the NIR region (800−950 nm) with lasing threshold of nearly 500 μW. Enhanced multiple scattering because of Au/ZnO disordered structure, exciton−plasmon coupling because of Au NPs, and enhanced charge transfer from ZnO to thick MoS_2 could be the possible reasons for RL in the above HS. The present work opens up new dimensions

DOI: 10.1021/acsomega.8b01287
ACS Omega 2018, 3, 14097−14102

toward realization of low power on-chip NIR random lasers made up of biocompatible materials.

■ ASSOCIATED CONTENT

Supporting Information

The Supporting Information is available free of charge on the ACS Publications website at DOI: 10.1021/acsomega.8b01287.

Detailed description about the experimental methods and additional characterizations (PDF)

■ AUTHOR INFORMATION

Corresponding Authors

*E-mail: klganapathi@iitm.ac.in (K.L.G.).
*E-mail: pnayak@iitm.ac.in (P.K.N.).
*E-mail: msrrao@iitm.ac.in (M.S.R.R.).

ORCID

Pramoda K. Nayak: 0000-0002-2569-0517

Notes

The authors declare no competing financial interest.

■ ACKNOWLEDGMENTS

This work was partially supported by Department of Science and Technology (DST) that led to the establishment of Nano Functional Materials Technology Centre (NFMTC) (SR/NM/NAT/02-2005). P.K.N. acknowledge the financial support from Department of Science and Technology, India, with sanction order no. SERB/F/5379/2017−2018 under Ramanujan Fellowship. K.L.G. acknowledge the financial support from Department of Science and Technology, India, with sanction order no. DST/INSPIRE/04/2016/001865 under DST INSPIRE Faculty program. T.D. would like to thank IIT Madras for proving institute postdoctoral fellowship.

■ REFERENCES

(1) Wiersma, D. S. Disordered Photonics. *Nat. Photonics* **2013**, *7*, 188−196.
(2) Luan, F.; Gu, B.; Gomes, A. S. L.; Yong, K.-T.; Wen, S.; Prasad, P. N. Lasing in Nanocomposite Random Media. *Nano Today* **2015**, *10*, 168−192.
(3) Cao, H.; Jiang, X.; Ling, Y.; Xu, J. Y.; Soukoulis, C. M. Mode Repulsion and Mode Coupling in Random Lasers. *Phys. Rev. B: Condens. Matter Mater. Phys.* **2003**, *67*, 161101.
(4) Abiyasa, A. P.; Yu, S. F.; Lau, S. P.; Leong, E. S. P.; Yang, H. Y. Enhancement of Ultraviolet Lasing from Ag-Coated Highly Disordered ZnO Films by Surface-Plasmon Resonance. *Appl. Phys. Lett.* **2007**, *90*, 231106.
(5) Fallert, J.; Dietz, R. J. B.; Sartor, J.; Schneider, D.; Klingshirn, C.; Kalt, H. Co-Existence of Strongly and Weakly Localized Random Laser Modes. *Nat. Photonics* **2009**, *3*, 279−282.
(6) Wiersma, D. S. The Physics and Applications of Random Lasers. *Nat. Phys.* **2008**, *4*, 359−367.
(7) Zhu, H.; Shan, C.-X.; Zhang, J.-Y.; Zhang, Z.-Z.; Li, B.-H.; Zhao, D.-X.; Yao, B.; Shen, D.-Z.; Fan, X.-W.; Tang, Z.-K.; et al. Low-Threshold Electrically Pumped Random Lasers. *Adv. Mater.* **2010**, *22*, 1877−1881.
(8) Krämmer, S.; Vannahme, C.; Smith, C. L. C.; Grossmann, T.; Jenne, M.; Schierle, S.; Jørgensen, L.; Chronakis, I. S.; Kristensen, A.; Kalt, H. Random-Cavity Lasing from Electrospun Polymer Fiber Networks. *Adv. Mater.* **2014**, *26*, 8096−8100.
(9) Wang, X.; Liao, Q.; Li, H.; Bai, S.; Wu, Y.; Lu, X.; Hu, H.; Shi, Q.; Fu, H. Near-Infrared Lasing from Small-Molecule Organic Hemispheres. *J. Am. Chem. Soc.* **2015**, *137*, 9289−9295.
(10) Wirths, S.; Mayer, B. F.; Schmid, H.; Sousa, M.; Gooth, J.; Riel, H.; Moselund, K. E. Room-Temperature Lasing from Monolithically Integrated GaAs Microdisks on Silicon. *ACS Nano* **2018**, *12*, 2169−2175.
(11) Wang, X.; Li, Z.-Z.; Zhuo, M.-P.; Wu, Y.; Chen, S.; Yao, J.; Fu, H. Tunable Near-Infrared Organic Nanowire Nanolasers. *Adv. Funct. Mater.* **2017**, *27*, 1703470.
(12) Cheng, R.; Li, D.; Zhou, H.; Wang, C.; Yin, A.; Jiang, S.; Liu, Y.; Chen, Y.; Huang, Y.; Duan, X. Electroluminescence and Photocurrent Generation from Atomically Sharp WSe_2/MoS_2 Heterojunction P − N Diodes. *Nano Lett.* **2014**, *14*, 5590−5597.
(13) Glazov, M. M.; Ivchenko, E. L.; Wang, G.; Amand, T.; Marie, X.; Urbaszek, B.; Liu, B. L. Spin and Valley Dynamics of Excitons in Transition Metal Dichalcogenide Monolayers. *Phys. Status Solidi B* **2015**, *252*, 2349−2362.
(14) Lagarde, D.; Bouet, L.; Marie, X.; Zhu, C. R.; Liu, B. L.; Amand, T.; Tan, P. H.; Urbaszek, B. Carrier and Polarization Dynamics in Monolayer MoS_2. *Phys. Rev. Lett.* **2014**, *112*, 047401.
(15) Mak, K. F.; He, K.; Shan, J.; Heinz, T. F. Control of valley polarization in monolayer MoS2 by optical helicity. *Nat. Nanotechnol.* **2012**, *7*, 494−498.
(16) Mai, C.; Barrette, A.; Yu, Y. Many-Body E Ff Ects in Valleytronics: Direct Measurement of Valley Lifetimes in Single-Layer MoS_2. *Nano Lett.* **2013**, *14*, 202−206.
(17) Radisavljevic, B.; Radenovic, A.; Brivio, J.; Giacometti, V.; Kis, A. Single-layer MoS_2 transistors. *Nat. Nanotechnol.* **2011**, *6*, 147−150.
(18) Nayak, P. K.; Horbatenko, Y.; Ahn, S.; Kim, G.; Lee, J.-U.; Ma, K. Y.; Jang, A.-R.; Lim, H.; Kim, D.; Ryu, S.; et al. Probing Evolution of Twist-Angle-Dependent Interlayer Excitons in $MoSe_2/WSe_2$ van der Waals Heterostructures. *ACS Nano* **2017**, *11*, 4041−4050.
(19) Nayak, P. K.; Lin, F.-C.; Yeh, C.-H.; Huang, J.-S.; Chiu, P.-W. Robust room temperature valley polarization in monolayer and bilayer WS_2. *Nanoscale* **2016**, *8*, 6035−6042.
(20) Splendiani, A.; Sun, L.; Zhang, Y.; Li, T.; Kim, J.; Chim, C.-Y.; Galli, G.; Wang, F. Emerging Photoluminescence in Monolayer MoS_2. *Nano Lett.* **2010**, *10*, 1271−1275.
(21) Mak, K. F.; Lee, C.; Hone, J.; Shan, J.; Heinz, T. F. Atomically Thin MoS_2: A New Direct-Gap Semiconductor. *Phys. Rev. Lett.* **2010**, *105*, 136805.
(22) Dhall, R.; Neupane, M. R.; Wickramaratne, D.; Mecklenburg, M.; Li, Z.; Moore, C.; Lake, R. K.; Cronin, S. Direct Bandgap Transition in Many-Layer $MoS_2$by Plasma-Induced Layer Decoupling. *Adv. Mater.* **2015**, *27*, 1573−1578.
(23) Li, Z.; Ezhilarasu, G.; Chatzakis, I.; Dhall, R.; Chen, C.-C.; Cronin, S. B. Indirect Band Gap Emission by Hot Electron Injection in Metal/MoS_2 and Metal/WSe_2 Heterojunctions. *Nano Lett.* **2015**, *15*, 3977−3982.
(24) Ganatra, R.; Zhang, Q. Few-Layer MoS_2: A Promising Layered Semiconductor. *ACS Nano* **2014**, *8*, 4074−4099.
(25) Ye, Y.; Wong, Z. J.; Lu, X.; Ni, X.; Zhu, H.; Chen, X.; Wang, Y.; Zhang, X. Monolayer Excitonic Laser. *Nat. Photonics* **2015**, *9*, 733−737.
(26) Salehzadeh, O.; Djavid, M.; Tran, N. H.; Shih, I.; Mi, Z. Optically Pumped Two-Dimensional MoS_2 Lasers Operating at Room-Temperature. *Nano Lett.* **2015**, *15*, 5302−5306.
(27) Li, Y.; Xu, H.; Liu, W.; Yang, G.; Shi, J.; Liu, Z.; Liu, X.; Wang, Z.; Tang, Q.; Liu, Y. Enhancement of Exciton Emission from Multilayer MoS_2 at High Temperatures: Intervalley Transfer versus Interlayer Decoupling. *Small* **2017**, *13*, 1700157.
(28) Chou, S. S.; Kaehr, B.; Kim, J.; Foley, B. M.; De, M.; Hopkins, P. E.; Huang, J.; Brinker, C. J.; Dravid, V. P. Chemically Exfoliated MoS_2as Near-Infrared Photothermal Agents. *Angew. Chem., Int. Ed.* **2013**, *52*, 4160−4164.
(29) Tsukazaki, A.; Ohtomo, A.; Onuma, T.; Ohtani, M.; Makino, T.; Sumiya, M.; Ohtani, K.; Chichibu, S. F.; Fuke, S.; Segawa, Y.; et al. Repeated Temperature Modulation Epitaxy for P-Type Doping and Light-Emitting Diode Based on ZnO. *Nat. Mater.* **2005**, *4*, 42−46.
(30) Xu, S.; Xu, C.; Liu, Y.; Hu, Y.; Yang, R.; Yang, Q.; Ryou, J.-H.; Kim, H. J.; Lochner, Z.; Choi, S.; et al. Ordered Nanowire Array

DOI: 10.1021/acsomega.8b01287
ACS Omega 2018, 3, 14097−14102

Blue/near-UV Light Emitting Diodes. *Adv. Mater.* **2010**, *22*, 4749−4753.
(31) Yang, Q.; Wang, W.; Xu, S.; Wang, Z. L. Enhancing Light Emission of ZnO Microwire-Based Diodes by Piezo-Phototronic Effect. *Nano Lett.* **2011**, *11*, 4012−4017.
(32) Dai, J.; Xu, C. X.; Sun, X. W. ZnO-Microrod/p-GaN Heterostructured Whispering-Gallery-Mode Microlaser Diodes. *Adv. Mater.* **2011**, *23*, 4115−4119.
(33) Chu, S.; Wang, G.; Zhou, W.; Lin, Y.; Chernyak, L.; Zhao, J.; Kong, J.; Li, L.; Ren, J.; Liu, J. Electrically Pumped Waveguide Lasing from ZnO Nanowires. *Nat. Nanotechnol.* **2011**, *6*, 506−510.
(34) Soci, C.; Zhang, A.; Xiang, B.; Dayeh, S. A.; Aplin, D. P. R.; Park, J.; Bao, X. Y.; Lo, Y. H.; Wang, D. ZnO Nanowire UV Photodetectors with High Internal Gain. *Nano Lett.* **2007**, *7*, 1003−1009.
(35) Bie, Y.-Q.; Liao, Z.-M.; Zhang, H.-Z.; Li, G.-R.; Ye, Y.; Zhou, Y.-B.; Xu, J.; Qin, Z.-X.; Dai, L.; Yu, D.-P. Self-Powered, Ultrafast, Visible-Blind UV Detection and Optical Logical Operation Based on ZnO/GaN Nanoscale P-N Junctions. *Adv. Mater.* **2011**, *23*, 649−653.
(36) Retamal, J. R. D.; Chen, C.-Y.; Lien, D.-H.; Huang, M. R. S.; Lin, C.-A.; Liu, C.-P.; He, J.-H. Concurrent Improvement in Photogain and Speed of a Metal Oxide Nanowire Photodetector through Enhancing Surface Band Bending via Incorporating a Nanoscale Heterojunction. *ACS Photonics* **2014**, *1*, 354−359.
(37) Dixit, T.; Palani, I. A.; Singh, V. Insights into Non-Noble Metal Based Nanophotonics: Exploration of Cr-Coated ZnO Nanorods for Optoelectronic Applications. *RSC Adv* **2018**, *8*, 6820−6833.
(38) Dixit, T.; Kumar, A.; Palani, I. A.; Singh, V. Surface-plasmon-mediated red and near infrared emission from Au-coated ZnO/$ZnCr_2O_4$ nanocomposites. *Scr. Mater.* **2016**, *114*, 84−87.
(39) Liu, W. Z.; Xu, H. Y.; Wang, C. L.; Zhang, L. X.; Zhang, C.; Sun, S. Y.; Ma, J. G.; Zhang, X. T.; Wang, J. N.; Liu, Y. C. Enhanced Ultraviolet Emission and Improved Spatial Distribution Uniformity of ZnO Nanorod Array Light-Emitting Diodes via Ag Nanoparticles Decoration. *Nanoscale* **2013**, *5*, 8634−8639.
(40) Kim, M. S.; Roy, S.; Lee, J.; Kim, B. G.; Kim, H.; Park, J.-H.; Yun, S. J.; Han, G. H.; Leem, J.-Y.; Kim, J. Enhanced Light Emission from Monolayer Semiconductors by Forming Heterostructures with ZnO Thin Films. *ACS Appl. Mater. Interfaces* **2016**, *8*, 28809−28815.
(41) Chen, L.; Xue, F.; Li, X.; Huang, X.; Wang, L.; Kou, J.; Wang, Z. L. Strain-Gated Field Effect Transistor of a MoS_2-ZnO 2D-1D Hybrid Structure. *ACS Nano* **2016**, *10*, 1546−1551.
(42) Zhang, K.; Zhang, Y.; Zhang, T.; Dong, W.; Wei, T.; Sun, Y.; Chen, X.; Shen, G.; Dai, N. Vertically coupled ZnO nanorods on MoS_2 monolayers with enhanced Raman and photoluminescence emission. *Nano Res.* **2015**, *8*, 743−750.
(43) Nazir, G.; Khan, M. F.; Akhtar, I.; Akbar, K.; Gautam, P.; Noh, H.; Seo, Y.; Chun, S.-H.; Eom, J. Enhanced photoresponse of ZnO quantum dot-decorated MoS_2 thin films. *RSC Adv.* **2017**, *7*, 16890−16900.
(44) Hsiao, Y.-J.; Fang, T.-H.; Ji, L.-W.; Yang, B.-Y. Red-Shift Effect and Sensitive Responsivity of MoS2/ZnO Flexible Photodetectors. *Nanoscale Res. Lett.* **2015**, *10*, 443.
(45) Jeong, H.; Oh, H. M.; Gokarna, A.; Kim, H.; Yun, S. J.; Han, G. H.; Jeong, M. S.; Lee, Y. H.; Lerondel, G. Integrated Freestanding Two-Dimensional Transition Metal Dichalcogenides. *Adv. Mater.* **2017**, *29*, 1700308.
(46) Zhao, W.; Ribeiro, R. M.; Toh, M.; Carvalho, A.; Kloc, C.; Castro Neto, A. H.; Eda, G. Origin of Indirect Optical Transitions in Few-Layer MoS_2, WS_2, and WSe_2. *Nano Lett.* **2013**, *13*, 5627−5634.
(47) Buscema, M.; Steele, G. A.; van der Zant, H. S. J.; Castellanos-Gomez, A. The Effect of the Substrate on the Raman and Photoluminescence Emission of Single-Layer MoS_2. *Nano Res.* **2014**, *7*, 561−571.
(48) Drüppel, M.; Deilmann, T.; Krüger, P.; Rohlfing, M. Diversity of Trion States and Substrate Effects in the Optical Properties of an MoS_2 Monolayer. *Nat. Commun.* **2017**, *8*, 2117.
(49) Li, H.; Zhang, Q.; Yap, C. C. R.; Tay, B. K.; Edwin, T. H. T.; Olivier, A.; Baillargeat, D. From Bulk to Monolayer MoS_2: Evolution of Raman Scattering. *Adv. Funct. Mater.* **2012**, *22*, 1385−1390.
(50) Gołasa, K.; Grzeszczyk, M.; Bożek, R.; Leszczyński, P.; Wysmołek, A.; Potemski, M.; Babiński, A. Resonant Raman Scattering in MoS_2- From Bulk to Monolayer. *Solid State Commun.* **2014**, *197*, 53−56.
(51) Li, Z.; Xiao, Y.; Gong, Y.; Wang, Z.; Kang, Y.; Zu, S.; Ajayan, P. M.; Nordlander, P.; Fang, Z. Active Light Control of the MoS2 Monolayer Exciton Binding Energy. *ACS Nano* **2015**, *9*, 10158−10164.
(52) Djurišić, A. B.; Leung, Y. H. Optical Properties of ZnO Nanostructures. *Small* **2006**, *2*, 944−961.
(53) Dixit, T.; Bilgaiyan, A.; Palani, I. A.; Nakamura, D.; Okada, T.; Singh, V. Influence of Potassium Permanganate on the Anisotropic Growth and Enhanced UV Emission of ZnO Nanostructures Using Hydrothermal Process for Optoelectronic Applications. *J. Sol-Gel Sci. Technol.* **2015**, *75*, 693−702.
(54) Maier, S. A.; Kik, P. G.; Atwater, H. A.; Meltzer, S.; Harel, E.; Koel, B. E.; Requicha, A. A. G. Local Detection of Electromagnetic Energy Transport below the Diffraction Limit in Metal Nanoparticle Plasmon Waveguides. *Nat. Mater.* **2003**, *2*, 229−232.
(55) Brown, A. M.; Sundararaman, R.; Narang, P.; Goddard, W. A.; Atwater, H. A. Nonradiative Plasmon Decay and Hot Carrier Dynamics: Effects of Phonons, Surfaces, and Geometry. *ACS Nano* **2016**, *10*, 957−966.
(56) Museum, B.; Dame, N.; Atwater, H. A Small World Full of Opportunities. *Nat. Mater.* **2010**, *9*, 181.
(57) Andreasen, J.; Asatryan, A. A.; Botten, L. C.; Byrne, M. A.; Cao, H.; Ge, L.; Labonté, L.; Sebbah, P.; Stone, A. D.; Türeci, H. E.; et al. Modes of Random Lasers. *Adv. Opt. Photon.* **2010**, *3*, 88−127.
(58) Van Der Molen, K. L.; Tjerkstra, R. W.; Mosk, A. P.; Lagendijk, A. Spatial Extent of Random Laser Modes. *Phys. Rev. Lett.* **2007**, *98*, 143901.
(59) Haglund, R. F.; Lawrie, B. J.; Mu, R. Coupling of Photoluminescent Centers in ZnO to Localized and Propagating Surface Plasmons. *Thin Solid Films* **2010**, *518*, 4637−4643.

DOI: 10.1021/acsomega.8b01287
ACS Omega 2018, 3, 14097−14102